Malaysian Journal of Analytical Sciences (MJAS)
Published by Malaysian Analytical Sciences Society

MOLECULAR DYNAMICS SIMULATION OF DTPA WITH $CaCO_3$ and FeS

(Simulasi Dinamik Molekul DTPA Dengan $CaCO_3$ dan FeS)

Abu Zar Che Azimi, Norhayati Abdullah* and Fatmawati Adam*

Faculty of Chemical and Process Engineering Technology, Universiti Malaysia Pahang Al-Sultan Abdullah, Lebuh Persiaran Tun Khalil Yaakob, 26300 Kuantan, Pahang, Malaysia

**Corresponding author: yatiabdullah@umpsa.edu.my, fatmawati@umpsa.edu.my*

Received: 8 December 2023; Accepted: 2 June 2024; Published: 27 August 2024

Abstract

In the production of oil and gas, calcium carbonate ($CaCO_3$) and iron sulphide (FeS) are among mineral scale deposits mainly found in tubing and valves located at surface facilities, which have been a nuisance in the oil flow during processing. Diethylenetriaminepentaacetic acid (DTPA) has a greater affinity to form stable divalent metal ion complexes during chelation to facilitate the dissolution of oilfield solid scale. Octadentate DTPA chelating ligand occupies five carboxylic acids, and three amine groups provide potential binding sites. The interaction between the molecules in the system can be replicated through molecular dynamics simulation explicitly using a COMPASS force field and the Ewald summation method available in the Material Studio software. The radial distribution function (RDF) in simulation trajectory files was utilised to study intermolecular interactions. The RDF results showed strong hydrogen bonding between O—H_2O and H_5—DTPA at a distance of 1.75 Å. The intermolecular interaction of DTPA with H_2O in the existing $CaCO_3$ and FeS denotes the interaction shift from water to the metal ion. The carbonyl group of DTPA exhibited a more significant interaction at a radial distance of 2.25 Å and intensity of 8.81 for Fe^{2+} but lower in $Ca^{2+,}$ which is at 1.47. The amine in DTPA analysis confirmed the low intensity of $CaCO_3$ at a distance of 5.75 Å and intensity of 1.07, and a distance of 2.25 Å and intensity of 1.01 for FeS. Meanwhile, amines in DTPA—CO_3^{2-} and DTPA—S^{2-} systems demonstrated the low interaction at the same distance of 4.75 Å. The interaction of Ca^{2+} with CO_3^{2-} in the DTPA system exhibited a sharp peak and high-intensity interaction at a distance of 2.25 Å and 13.71 intensity. Nevertheless, a sharp and low-intensity peak appeared on the Fe^{2+}—S^{2-} in the DTPA system at a distance of 4.75 Å and 2.18 intensity. In conclusion, these findings suggest that the carbonyl group of DTPA has a stronger interaction with Fe^{2+} than Ca^{2+}. Meanwhile, the hydroxyl group of DTPA shows the highest intensity of interaction with CO_3^2. Additionally, Ca^{2+} ions form more significant interactions with CO_3^{2-} ions in the DTPA systems.

Keywords: diethylenetriaminepentaacetic acid, radial distribution function, molecular dynamics simulation, compass, calcium carbonate

Abstrak

Dalam pengeluaran minyak dan gas, kalsium karbonat ($CaCO_3$) dan besi sulfida (FeS) ialah mendapan kerak mineral yang boleh didapati terutamanya dalam tiub dan injap yang berada di kemudahan permukaan dan menyebabkan gangguan dalam aliran minyak semasa pemprosesan. Asid diethylenetriaminepentaasetik (DTPA) mempunyai afiniti yang lebih tertarik untuk membentuk kestabilan untuk kompleks ion logam divalen semasa pengkelatan untuk memudahkan pelarutan kerak pepejal medan minyak. Oktadentat ligan pengkelat DTPA menduduki lima asid karboksilik, dan tiga kumpulan amina menyediakan tapak pengikatan yang

berpotensi. Interaksi antara molekul dalam sistem boleh direplikasi melalui simulasi dinamik molekul secara jelas menggunakan medan daya COMPASS dan kaedah penjumlahan Ewald yang tersedia dalam perisian Material Studio. Fungsi pengedaran jejari (RDF) dalam fail trajektori simulasi telah digunakan untuk mengkaji interaksi antara molekul. Keputusan fungsi taburan jejari menunjukkan ikatan hidrogen yang kuat antara O—H_2O dengan H_5—DTPA pada jarak jejari 1.75 Å. Interaksi antara molekul DTPA dengan H_2O dalam $CaCO_3$ dan FeS sedia ada menandakan peralihan interaksi daripada air ke ion logam. Kumpulan karbonil DTPA menemui interaksi yang lebih ketara pada jarak 2.25 Å dan keamatan 8.81 untuk Fe^{2+} tetapi lebih rendah untuk Ca^{2+}, iaitu pada 1.47. Amina dalam analisis DTPA mengesahkan keamatan rendah $CaCO_3$ pada jarak 5.75 Å dan keamatan 1.07, manakala FeS pada jarak 2.25 Å dan keamatan 1.01. Sementara itu, amina dalam sistem DTPA—CO_3^{2-} dan DTPA—S^{2-} menggambarkan interaksi rendah pada jarak yang sama iaitu 4.75 Å. Ca^{2+}—CO_3^{2-} dalam sistem DTPA menunjukkan interaksi puncak yang tajam dan berintensiti tinggi pada jarak 2.25 Å dan keamatan 13.71. Namun begitu, puncak tajam dan keamatan rendah muncul pada Fe^{2+}—S^{2-} dalam sistem DTPA pada jarak 4.75 Å dan keamatan 2.18. Secara keseluruhan, penemuan ini menunjukkan bahawa kumpulan karbonil DTPA mempunyai interaksi yang lebih kuat dengan ion Fe^{2+}. Kumpulan hidroksil DTPA menunjukkan interaksi intensiti tertinggi dengan CO_3^{2-}. Selain itu, ion Ca^{2+} membentuk interaksi yang lebih signifikan dengan ion CO_3^{2-} dalam sistem DTPA.

Kata kunci: asid diethylenetriaminepentaasetik, fungsi taburan jejari, simulasi dinamik molekul, COMPASS, kalsium karbonat

Introduction

Oilfield solid scale accumulation in petroleum pipelines, which generates flow control issues while transferring crude oil and natural gas, has agained a research focus [1]. Scale formation in oil and gas pipeline networks creates the conditions for various possible disasters. Among them include valves faltering in their duty, flow succumbing to restrictive barriers, equipment suffering the scars of damage, and the corrosion of pipes or the concealed erosion of tube surfaces beneath the scale [2]. Calcium carbonate ($CaCO_3$) scale is one of the primary prevalent solid scales, particularly in tube wells [3]. The precipitation of $CaCO_3$ occurs when a conversion in temperature and pressure causes the discharge of dissolved carbon dioxide (CO_2) from aqueous to gaseous form from the circulating fluid [4, 5]. A real-scale sample revealed the presence of calcium ions (Ca^{2+}) in the precipitated silica sand solid scale of an oil well. Other elements like oxygen (O), aluminium (Al), and iron (Fe) are present in the complex combination of metal elements [6]. Meanwhile, hydrogen sulphide and iron reaction produce iron sulphide (FeS) scales [7]. Bacterial activity, thermal degradation of sulphate, and gas lift activities are the sources of hydrogen sulphide [8, 9]. Scaling or dissolving scales is accomplished using mechanical or chemical handling [10]. Nevertheless, the mechanical approach is costly and unreliable when the solid scale is difficult to retrieve and might harm the tubing [11, 12]. An inappropriate chemical selection in the cleaning procedure will accelerate the scale return and deteriorate pipe corrosion. Recently, chelating agents have been an attractive and viable alternative to organic and inorganic acids for scale removal. Chelating compounds are less corrosive to well tubes, tubular, and other downhole tools, readily biodegradable, and more ecologically friendly [13]. Chelating agents have an extremely minimal corrosion rate compared to hydrochloric acid, which is their primary attraction [14]. Fewer corrosion inhibitors are needed as there is less corrosion [15, 16]. Chelating agents with carboxylic and amine functional groups are the most prevalent dissolvers and inhibitors in solid scale dissolution [17].

This study modelled the molecular interactions associated with the dissolution of ($CaCO_3$) and iron sulphide (FeS) utilising diethylenetriaminepentaacetic acid (DTPA). For a dissolution solvent, it is essential to comprehend how the functional groups of the dissolver and the solid scale interact at the molecular level. This can give molecular insights that are used to predict how the solid scale and the solvent of interest will interact. Currently, simulation work for chelating agents and solid scale interactions is still lacking; thus, molecular dynamics simulation is required as an approach to better understand the capability of chelating agents to interact with solid scale. An intense intermolecular interaction between the functional groups of the chelating agent reflects good solid scale removal. DTPA is an octodentate ligand where three amines and five carboxylic groups can form a more stable metal-ion complex [18]. It has impressive formation constants

among the several chelating agents utilised in the petroleum industry. Synthesis and evaluation of glutamic acid hydrochloride as a potential dissolver for $CaCO_3$ exceeded 3,000 ppm dissolution at low concentrations [19]. The simulation showed a strong intermolecular interaction between the carbonyl group and Ca^{2+} ions in GLDA and Fe^{2+} ions in GLDA and GLDA-Na_4 [20]. Furthermore, according to the radial distribution function (RDF) analysis, there is evidence of hydrogen bonding between the solvent molecules and patchoulol solutes. The hydroxyl functional groups of patchoulol, specifically the oxygen atom (O1P) and hydrogen atom (H1P), played a significant role in this interaction [21].

Understanding the dissolution of solid scale removal is a crucial concern in oil and gas research. The reliance on experimental methods is insufficient for characterising the molecular-level interactions that impede the dissolution of a specific solid scale by a particular dissolver. Exploring different configurations at an atomic scale and dynamic processes, which are rigorously studied using simulation methods, are great tools for molecular dynamics modelling. The computational method known as molecular dynamics involves the treatment of atoms as individual particles that follow classical mechanics principles. This work applied molecular dynamics simulations to examine the interaction of DTPA with $CaCO_3$ and DTPA with FeS systems. The results feature improved dissolver formulas for creating new solid scale removal techniques with improved dissolution.

Materials and Methods

Molecular dynamics simulation

The exploration of atomic configuration and motion of molecules in solids and liquids is substantially aided by molecular dynamics techniques in computer simulations [22]. This method has shown to be a handy tool. The simulation of intermolecular interactions was performed using molecular dynamics simulations with the Accelrys Material Studio version 7.0 software provided by Accelrys, Inc., based in San Diego, USA. The simulation processes incorporated the Condensed-Phase Optimized Molecular Potentials for Atomistic Simulation Studies (COMPASS) force field in all instances. The processes were upgraded by incorporating the state-of-the-art-third-generation force fields, specifically the COMPASS [23]. The Verlet-velocity algorithm integrates the equations governing atomic motion numerically [24]. Separated pairs of atoms interact via the non-bonded interactions, which comprise a van der Waals (vdW) element expressed in an LJ-12-6 function and an electrostatic interaction described by a Coulombic function as per Equations (1) and (2), respectively [25, 26]. The three-dimensional structures of DTPA, $CaCO_3$, FeS, and H_2O molecules exploited in the simulation were downloaded from the ChemSpider database [27, 28, 29, 30, 31]. Table 1 summarises the total number of DTPA, $CaCO_3$, FeS, and H_2O molecules used in this research. The expression for energy in the COMPASS force field is readily summed up in Equation (3):

$$E_{vdw} = 4\varepsilon\left[\left[\frac{\sigma}{r}\right]^{12} - \left[\frac{\sigma}{r}\right]^{6}\right] \quad (1)$$

$$\sum_{i=1}^{N_A}\sum_{i=1}^{N_B}\frac{q_i q_j}{4\pi q_o r_{ij}} \quad (2)$$

$$E_{tot} = E_{bond} + E_{angle} + E_{torsion} + E_{\iota} + E_{cross} + E_{elec} + E_{LJ} \quad (3)$$

Using the COMPASS force field and the Smart algorithm, the molecular geometry was optimised for electrostatic and vdW interactions using an atom-based summation technique. This optimisation stage aimed to create a stable molecular geometry for the following stages of modelling and simulation. The simulation box was assembled utilising the Amorphous Cell module within the Material Studio software, encompassing the chelating agent (DTPA), solid scale $CaCO_3$/FeS, and water components, as illustrated in Figure 1. The system underwent minimisation using a 10,000-step (fine) Smart Minimizer. Molecular dynamics simulations were

organised by engaging the COMPASS force field and the Ewald-based summation method to account for electrostatic and vdW interactions [32, 33]. Ewald summation was employed to handle long-range electrostatic interactions [34]. The initial molecular dynamics simulation employed a microcanonical ensemble (NVE) for 1,000 ps, starting with a minor time step of 0.5 fs, and the time step was progressively increased in the early stages of the simulation to 1 fs. After that, the system was simulated for a further 1000 ps at a timestep of 1 fs using an isothermal-isobaric ensemble (NPT), which replicated the conditions in a well reservoir at 136 atm and 90°C. The temperature and pressure were maintained using Nose thermostats [35, 36, 37] and Berendsen barostats [38, 39]. Throughout the equilibration and dynamic steps, the trajectory file for each simulation system was recorded and saved every 100 ps.

Table 1. Details on the simulation parameters for the DTPA with $CaCO_3$ and DTPA with FeS intermolecular interaction systems

	Number of Molecules				Temperature,	Pressure (NPT),
System	**DTPA**	**$CaCO_3$**	**FeS**	**Water**	**°C**	**atm**
System 1	30	-	-	270	90	136
System 2	30	60	-	270	90	136
System 3	30	-	60	270	90	136

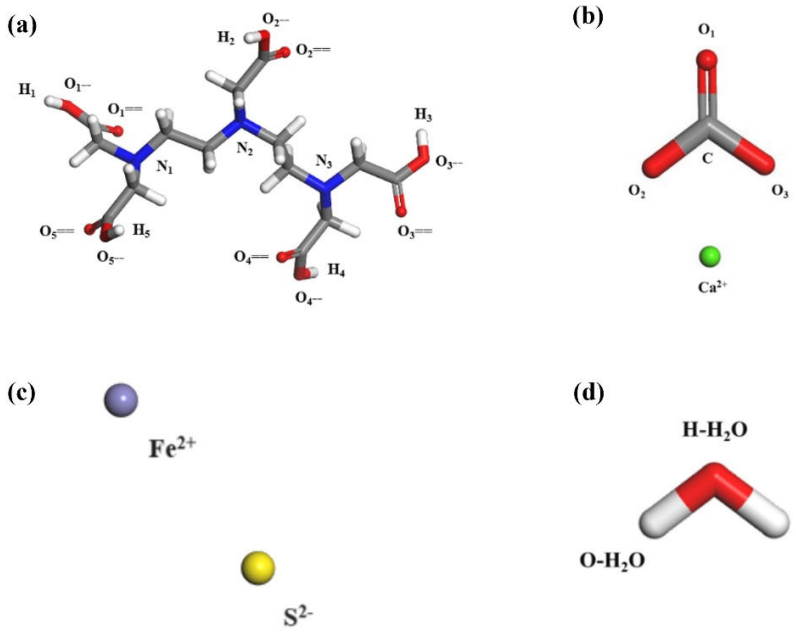

Figure 1. Diethylenetriaminepentaacetic acid (DTPA), Calcium carbonate ($CaCO_3$), Iron sulphide (FeS), Water (H_2O)

Radial distribution function analysis

The RDF was applied to the trajectory output file to examine the relationships between the assigned functional groups, which is presented in Equation (4):

$$g_{xy}(r) = \frac{\langle N_y\,(r,r+dr)\rangle}{\rho_r 4\pi r^2 dr} \quad (4)$$

where r is the radius, ρ_y is the density of the y atom, and N_y (r, r + dr) is the number of y atoms.

Figure 1 depicts the labelling of the compounds employed in this simulation for chemical recognition. The identification numbers for the carboxyl groups of the DTPA molecule were 1 to 5. The carboxylic groups of DTPA are more practically classified into two subgroups: hydroxyl and carbonyl. The oxygens in the hydroxyl groups of DTPA were designated as O_1—, O_2—, O_3—, O_4— and O_5—. The dash character (—) describes the single bond in the hydroxyl group. Meanwhile, H_1, H_2, H_3, H_4, and H_5 were assigned to hydrogens in the hydroxyl group. The carbonyl group oxygen atoms were regarded as O_1==, O_2==, O_3==, O_4==, and O_5==. The equals sign indicates the double bond in the carbonyl group (=). The amines in DTPA were identified as N_1—DTPA, N_2—DTPA, and N_3—DTPA. The calcium ion in $CaCO_3$ and the iron ion in iron (II) sulphide were represented by Ca^{2+} and Fe^{2+}, respectively. Three oxygen carbonate ions were labelled O_1, O_2, and O_3, whereas the sulphide ion was labelled S.

Results and Discussion

Investigating the interactions between a solvent and a solid surface at a molecular level is crucial. The strength of these interactions directly correlates with the solvent ability to dissolve the solid effectively. Therefore, in this research, the RDF was employed to model the interactions between neighbouring atoms to predict the extent of intermolecular interactions. Temperature plays an essential role in improving the efficiency of metal ion complexes as heat can render the attraction of metal ions with chelating agents, thus increasing the dissolution.

From Figure 2, the DTPA molecules are initially uniformly dispersed and surrounded by water molecules. The DTPA molecules are in an extended configuration, with their carboxylate and amine groups towards the aqueous environment. Following 1,000 ps simulation at constant pressure and temperature (NPT), the DTPA molecules exhibit aggregation, resulting in a uniformly distributed DTPA and H_2O. This behaviour reflects the dissolution of DTPA in H_2O.

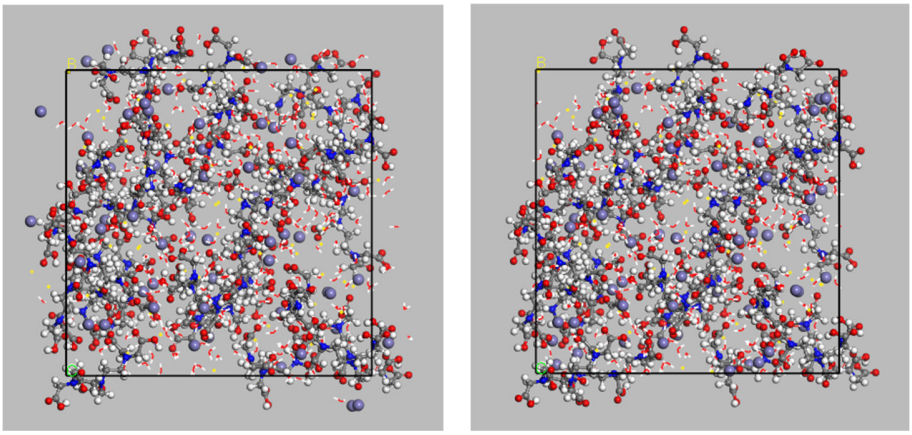

(a) Initial configuration (before simulation) (b) After simulation (NPT 1,000 ps)

Figure 2. Initial and final configurations of the DTPA—H_2O system

DTPA with H_2O

This section details the RDF plots illustrating water intermolecular interactions with the hydrogen and oxygen atoms within the carboxylic groups of DTPA. In DTPA with the water system, there is a strong intermolecular interaction between O—H_2O and H_5—DTPA at a distance of 1.75 Å and intensity of 2.57, with g(r) of 1.16 and 2.10 between H_1 and H_3 atoms, as shown in Figure 3. The first peak corresponds to the closest neighbour interaction between the specific types of atoms in DTPA solution, where the oxygen atoms of water show higher intensity interaction than hydrogen at a distance of 3.25 Å and 1.23 intensity. Therefore, the RDF pattern explains that the closest neighbouring interaction occurs between O—H_2O and H_5—DTPA atoms, representing strong hydrogen bonding in DTPA molecules [40, 41]. In addition, the effect of intramolecular hydrogen bonding in DTPA occurs

between a terminal acetate and a central nitrogen [42, 43]. The strength of these interactions can also be explained by water oxygen being more electronegative than hydrogen [44]. Apart from that, the hydrogen atoms of DTPA are bound to carbon and nitrogen atoms, which are less electronegative than oxygen [45, 46]. Meanwhile, the interaction still occurs for the remaining atoms of H_1 and H_3 but is lower than H_5—DTPA. At a range exceeding 9.25 Å, the intensity approaches 1.00, signifying the non-existence of long-range ordered interaction. The second peak displays a relatively weak contact between H—H_2O and O—DTPA, with a distance of 3.25 Å. An extended top curve with reduced intensity indicates that H—H_2O and O_5—DTPA interact with a g(r) value of 1.23. Both interaction results agree with the previously reported findings on the interaction of DTPA with water at 60 °C [47]. An expanded study that includes other polyaminocarboxylic acids, such as ethylenediaminetetraacetic acid and triethyl-enetetraminehexaacetic acid, is more comprehensive in demonstrating the hydrogen bonding effect. Specific evidence on the analysis for this chelating agent molecule has been proven in Raman, infrared, and nuclear magnetic resonance spectra [48, 49, 50]. Furthermore, this result implies that the sequence of the electronegativity between O-H of water and DTPA extensively agrees with the previous study [51].

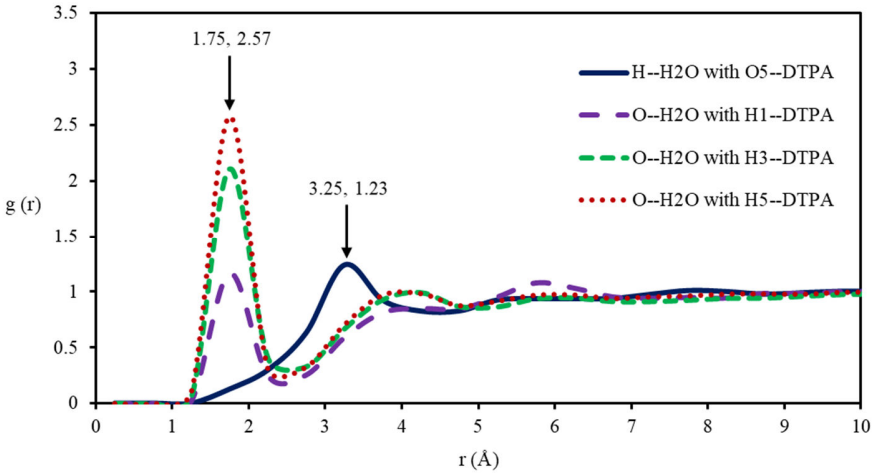

Figure 3. The g(r) plots of DTPA in water, intermolecular interactions in O--H_2O with H—DTPA and H—H_2O with O—DTPA

From Figure 4, DTPA molecules are initially disseminated randomly in an aqueous solution containing $CaCO_3$ surfaces. This dispersion phenomenon results from an extended molecule conformation, which introduces functional groups. Notable changes appear after 1,000 ps of constant pressure and temperature (NPT). The DTPA molecules on the $CaCO_3$ solid scale likely reflect the intermolecular interactions between DTPA-$CaCO_3$ molecules and water molecules.

DTPA with H_2O in the existing $CaCO_3$

This passage describes the outcome of the analysis of DTPA intermolecular interactions with water in the presence of $CaCO_3$ scale. The H_2O—DTPA interaction, namely O—H_2O with H_5—DTPA in the presence of $CaCO_3$, is shown in Figure 5. A slightly decreasing difference was detected between the O—H_2O and H_5—DTPA interaction patterns compared to Figure 6. The intensity dropped from 2.57 to 0.98 at a distance of 1.75 Å. The RDF pattern indicates that $CaCO_3$ has modified the shifting of O—DTPA with Ca^{2+} ions. This is because the O—DTPA molecule is self-stabilised on solute-solvent structures in the water. These changes also manifest the start of the chelation stage on metal ion complexes between the solvent molecules, DTPA, and solute molecules, $CaCO_3$, during dissolution. At a distance of 3.25 Å, the RDFs started to increase, and at

4, it started to fall. The intensity equals 1.00 for distances larger than 4, suggesting no long-range order exists, which indicates less of locating an interaction between hydroxyl water molecule and DTPA. An electrostatic interaction represents a long-range interaction, while a short-range interaction is signified by the vdW interaction between DTPA and H_2O. The adsorption energy of carboxymethyl inulin on calcite (104), (110), and (012) surfaces is primarily influenced by electrostatic interactions among charged atoms, hydrogen bonding, and vdW forces [52]. The discussion also addressed how the high adsorption energies of CO_2 on graphite are influenced by pore size and surface functional groups, employing both density functional theory and grand canonical Monte Carlo simulations [53]. The second peak, however, indicates a weak interaction between H—H_2O and O_5—DTPA, with a distance of 3.25 Å. By looking at a stretched top bend with moderate probability g(r) at 1.20, it is possible to demonstrate a slight difference in Figure 5.

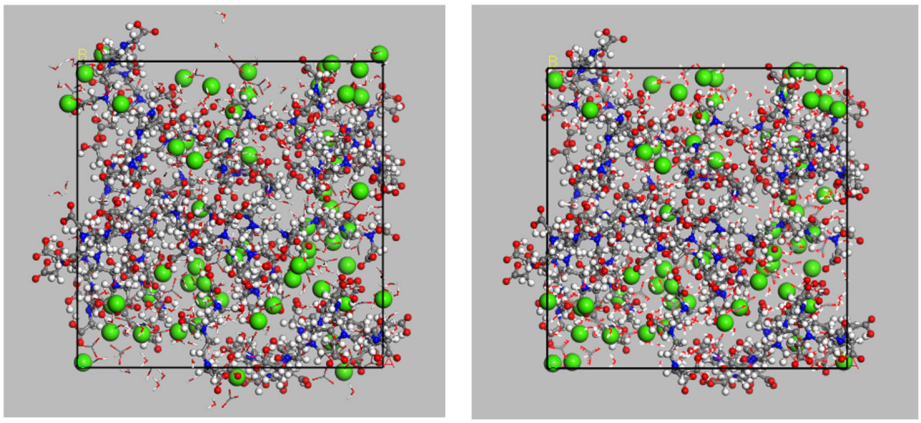

(a) Initial configuration (before simulation) (b) After simulation (NPT 1,000 ps)

Figure 4. Initial and final configuration of the DTPA—$CaCO_3$—H_2O system

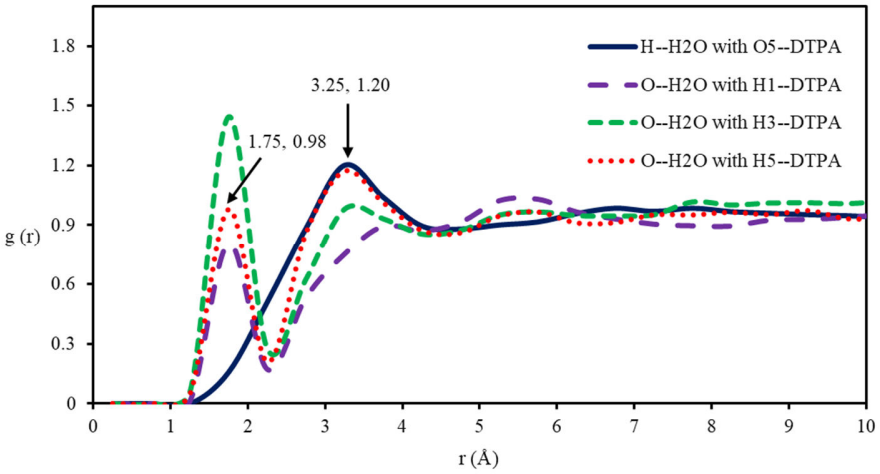

Figure 5. The g(r) plots of DTPA in water in $CaCO_3$ presence, intermolecular interactions in O—H_2O with H—DTPA and H—H_2O with O—DTPA

From Figure 6, in the first configuration of the DTPA—FeS—H_2O system, DTPA molecules expand conformation with exposed carboxylate and amine groups as they scatter randomly in the water with FeS surfaces. Following 1,000 ps simulation in a constant-pressure and temperature (NPT) ensemble, the DTPA

aggregates are formed and driven by interactions between DTPA and water molecules.

DTPA with H_2O in the existing FeS

Similar to the $CaCO_3$ interaction in Figure 8, the RDF for the interaction of DTPA with water in the existing FeS is demonstrated in Figure 7. Based on figure, the interactions between the hydrogen atoms of DTPA, which are H_1, H_3, and H_5, with the oxygen atoms in H_2O, are low, similar to all graph patterns. The distance is 3.25 Å with g(r) at 0.95 for H—H_2O with O_5—DTPA interaction. About 11.7% of the intensity value dropped significantly from 2.57 in water (Figure 6) to 0.30 for H_5—DTPA. Shifting in the water of the hydroxyl group to a lower intensity indicates bonding of the polarised O-H bond, possibly with the iron ion, Fe^{2+}. At an elevated temperature of 90 °C, this result is likely due to the weakening of hydrogen bonds between water molecules [54]. The reduction of RDF intensity affecting O-H and C=O functional groups signals the formation of a metal-ligand soluble complex [55]. Therefore, Fe^{2+} was chosen as the complex metal ion chelating with DTPA [56]. The RDF reveals the long-range disorder correlation between particles of all cases, as its values converge to 1.00 at distances greater than 4.75 Å. The non-bond interactions are used for interactions between DTPA and H_2O in the presence of FeS. It includes a Coulombic function for the electrostatic interaction and an LJ-9-6 function for the vdW term. Chemicals and rocks interact via a process known as adsorption, in which a chemical binds to the surface of a rock via vdW force interaction [57]. In addition, the Derjaguin-Landau-Verweye-Overbeek (DLVO) prediction of colloid stability has been cited in the literature to describe the adhesion phase in a fouling process. Other forms of contact, such as hydrophobic, steric, or ion bridging, can engage in addition to DLVO forces (vdW and electrostatic), and the net result is a mix of all the possible interactions [58].

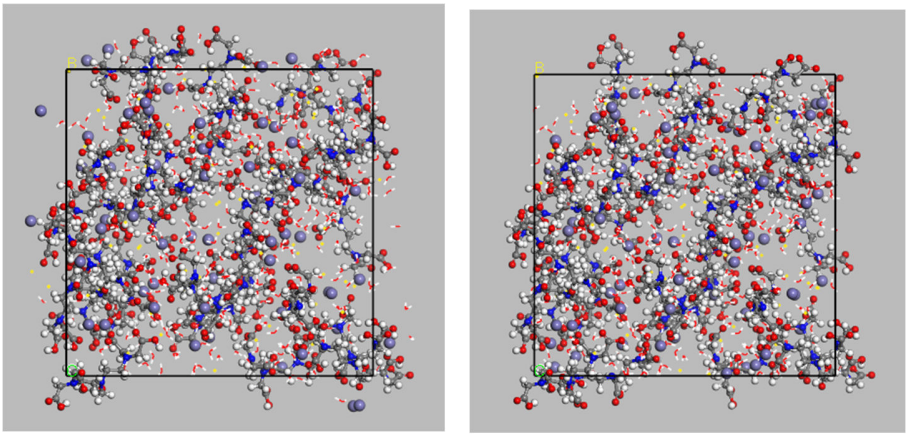

(a) Initial configuration (before simulation) (b) After simulation (NPT 1,000 ps)

Figure 6. Initial and final configuration of the DTPA—FeS—H_2O system

DTPA with (calcium or iron) ion

According to the literature, the metal ion complexes event will be characterised by strong intermolecular interactions associated with the sharp and closest radial distance peaks in g(r) [20]. Figure 8 (a) shows the carbonyl and hydroxyl of DTPA. The triple carbonyl, which is O_1==, O_3==, and O_5==, has more intensity interaction g(r) than hydroxyl. The O_5== shows the highest interaction with Ca^{2+} ion at a distance of 2.25 Å, 1.47. Meanwhile, the hydroxyl group shows the RDF point with minimal intensity at a distance of 3.75 Å, 1.51 for O_5—DTPA with Ca^{2+} interaction. Although the interactions at a distance of 2.25 Å in this simulation exhibit less strength associated with O—H_2O and H_5—DTPA interaction in Figure 6, specifically at the initial radial distance of 1.75 Å, the presence of an abundant hydroxyl group in DTPA is noteworthy. This abundance could facilitate hydrogen bond formation, serving as a hydrogen donor or acceptor. As part of the metal-ion complexes process, the hydroxyl group will lose its

proton, H^+, to oxygen, which can bind and hold on to the metal ion [20]. The hydroxyl group is deprotonated with a delocalised electron form on carboxylate ions [-COO] [60]. The correlation of the long-range fluctuations of carbonyl and hydroxyl waves within the interaction with Ca^{2+} is slow with distances, as demonstrated by the peak convergence of metal ion complexes from g(r) 5.25 to 1.00 Å.

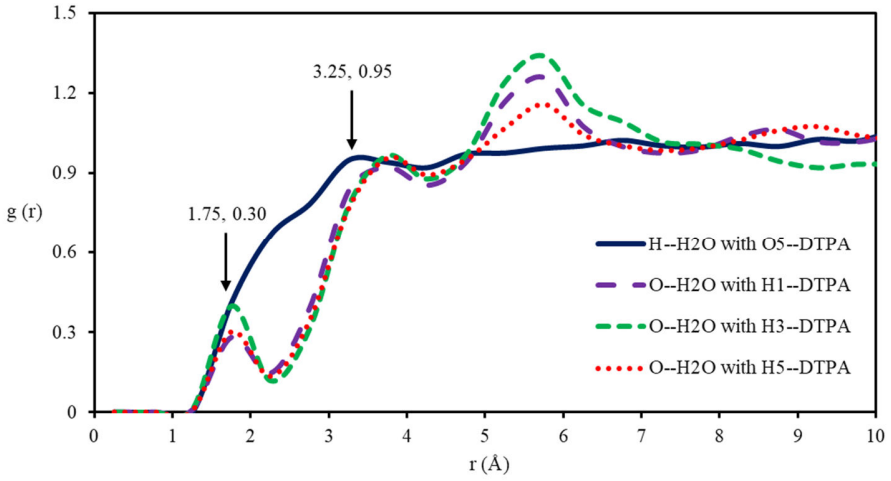

Figure 7. The g(r) plots of DTPA in water in FeS presence, intermolecular interactions in O—H_2O with H—DTPA and H—H_2O with O—DTPA

As shown in Figure 8 (b), the carbonyl group intermolecular interactions with iron are primarily significant. The first peak is identified at a distance of 2.25 Å with an intensity value of g(r) of 8.81 for the O_1==Fe^{2+} interaction. The interaction on O_3== and O_5== also shows the highest values at 7.87 and 7.90, respectively, close to O_1== intensity. The DTPA-iron interaction discloses that the carbonyl groups have more promising interactions than hydroxyl. The hydroxyl in the second peak demonstrates the broad peak, and low intensity occurs at a distance of 4.25 Å in the 2.26 – 2.65 range values. All interactions exhibit a straight line at the same point r, 4.75 Å. This simulation revealed that all carbonyls (C=O) in DTPA are more attracted to interacting with metal ions, $Fe^{2+,}$ than with H—(H_2O) in Figure 8 (b). The carboxylate groups (COO^-) in DTPA have a pair of electrons that form covalent bonds with the metal ion Fe^{2+}. The adsorbed H ions are expected to form associations with the sulphide ions of the lattice, which initiate the dissolution process [61]. The carbonyls interact on the surface at the iron lattice site and generate a charge disparity imbalance, leading to the extraction of Fe^{2+} from the FeS.

Amine in DTPA with (calcium, iron, carbonate, or sulphide) ion

Figure 9 (a) illustrates the RDF pattern depicting the intermolecular interaction between the amine functional group of DTPA and calcium ions. Three amines, N_1, N_2, and N_3, associated with DTPA exist at a distance of 5.75 Å. The findings of simulations reflect the low degree of intensity by intermolecular hydrogen bonding between amine and carboxylic groups. The results help justify the interaction of metal ions that tend to interact with the carbonyl in Figure 8 rather than the amines of DTPA itself in this simulation The DTPA carboxylic acid groups are linked to the chelating agent 'arms' and bind to calcium ions by 'grabbing' them from the solution [62]. In contrast, the nitrogen group is typically found at the molecule's centre. The study found that the metal ions in M(Glu), M(Asp), and some metal ions can form chelates over amine groups, leading to the selectivity of metal ions and their transfer through building complexes [63]. As an example, when there are positively charged amines, intramolecular hydrogen bonds are created (as seen in $C_3N\cdots H\cdots O_2C$), which can result in the acid groups of DTPA becoming unavailable for binding to barium sites on the surfaces of crystals [64].

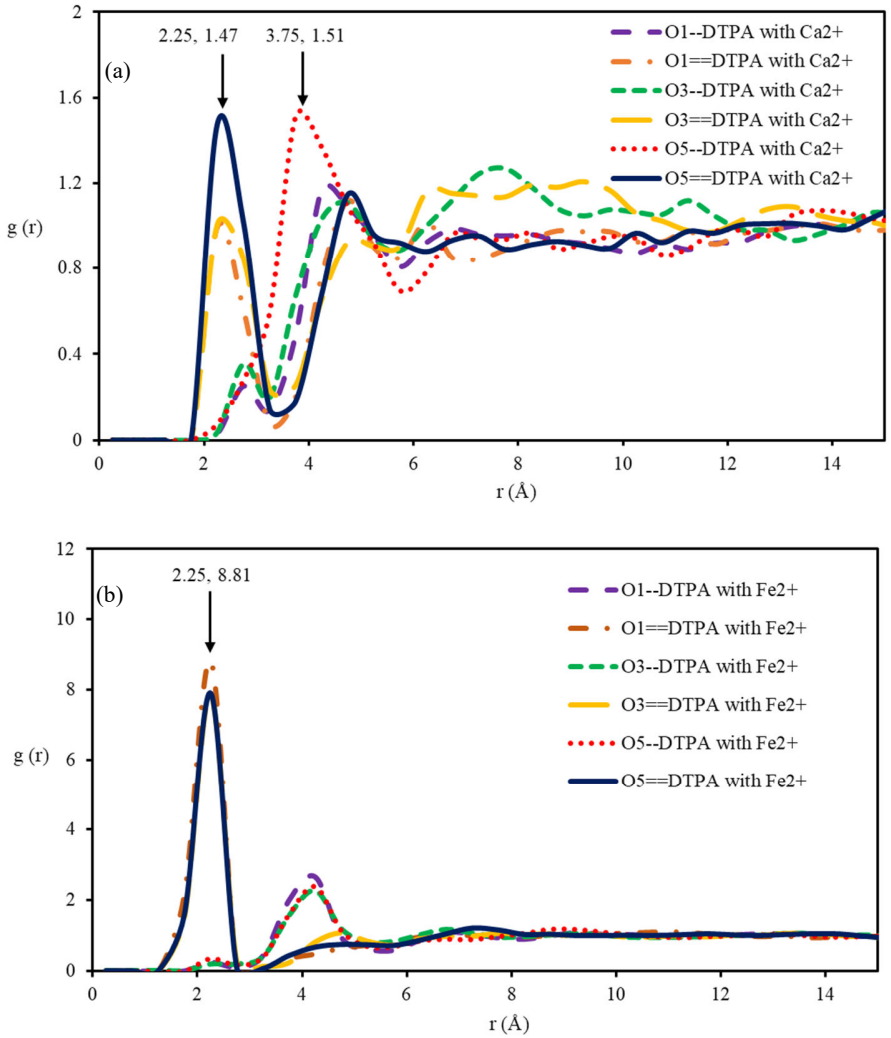

Figure 8. The g(r) plots of the DTPA carboxylic group with (a) Ca^{2+} and (b) Fe^{2+} ion.

Figure 9 (b) elucidates the RDF pattern describing the intermolecular interaction involving the amine functional group of DTPA with FeS. The association of amine, specifically N_1 in DTPA, was observed with a g(r) value of 1.01 for iron at a distance of 2.25 Å. The N_2 and N_3 also show higher g(r) values at 1.40 and 1.27, respectively, with the same distance. The findings of simulations reflect the low degree of intensity stimulated by the intermolecular hydrogen bonding between the carboxylic and amine groups in DTPA. Additionally, lone pairs of electrons are present in the nitrogen atoms of the amine groups (NH_2). Although these nitrogen atoms can engage in coordination chemistry, in the case of DTPA, the carboxylic acid groups are frequently linked to significant chelation sites in Figure 8.

In Figure 9 (c), the amine functional group has a weaker intermolecular interaction between carbonates. Compared to Figure 9 (a), amine favours calcium ions with more vital intermolecular interaction than carbonate ions The chelation of calcium ions by DTPA results in changes to the solubility of $CaCO_3$. Hydrogen bonding is a mechanism by which amine groups and carbonate ions interact. In the case of the amine group

of DTPA and the carbonate ion of $CaCO_3$, the amine group contains a nitrogen atom with a lone pair of electrons. The carbonate ion (CO_3^{2-}) has three oxygen atoms, and one carries a partial negative charge. These two charges, partially positive on the hydrogen atom in the amine group and partially negative on the oxygen atom in the carbonate ion, attract each other, creating the hydrogen bond.

In Figure 9 (d), the amine functional group has a weaker intermolecular interaction between sulphides. In comparison to Figure 9 (b), amine prefers iron with stronger intermolecular interaction. Amine groups are present in DTPA. Nitrogen (N) atoms bound to hydrogen (H) atoms comprise an amine group. As nitrogen only possesses two electrons that are not employed in bonds and are focused on the nitrogen atom, it is known as having a lone pair of electrons. The lone pair of electrons on the nitrogen is attracted to the partial positive charge on the hydrogen atom in the S—H bond of the sulphide ion.

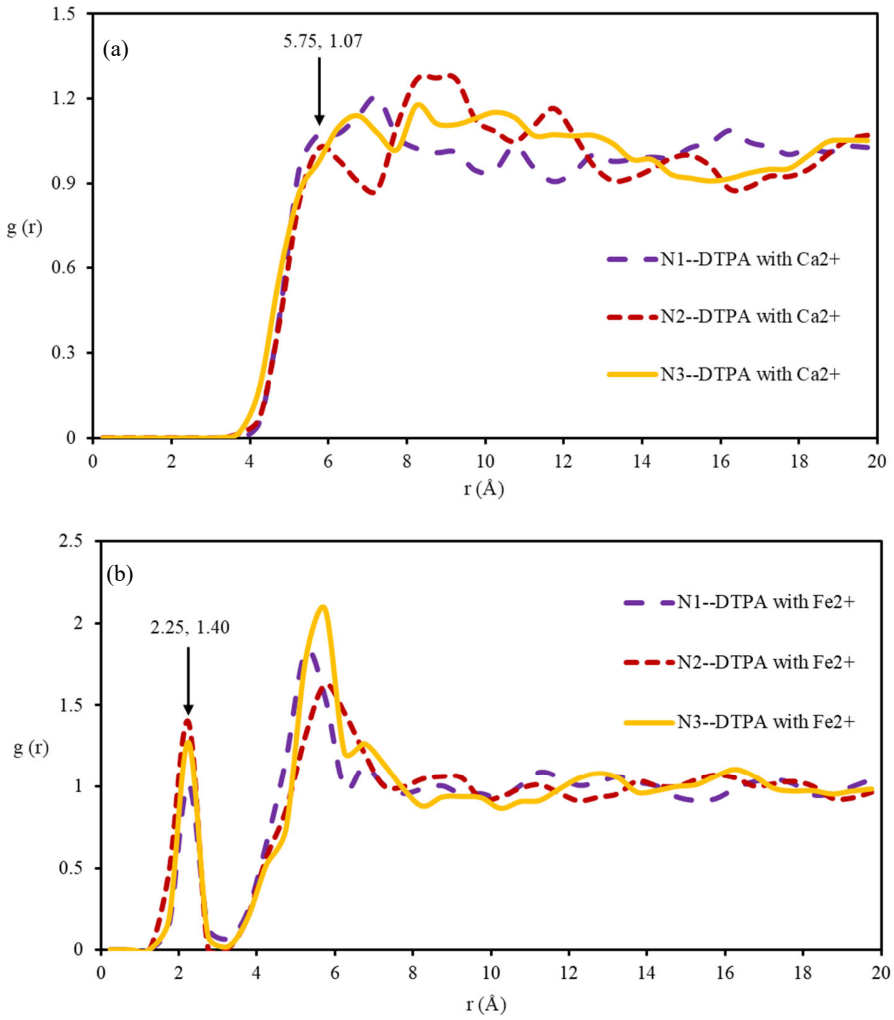

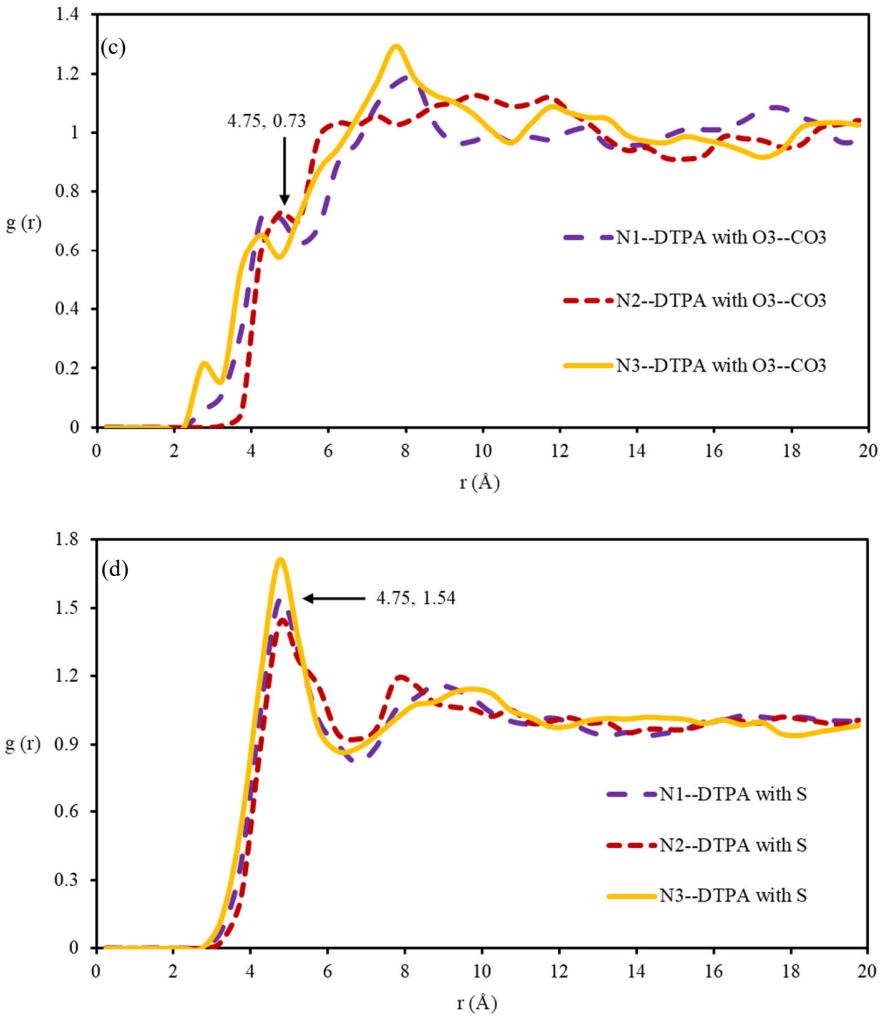

Figure 9. Interaction between the amine in DTPA and (a) Ca^{2+}, Fe^{2+}, (c) carbonate, O_3^{2-} ion of $CaCO_3^{2-}$ and (d) sulphide, S^{2-} ion of FeS

Calcium with carbonate ions in DTPA

Figure 10 shows the intermolecular interaction of Ca^{2+} with CO_3^{2-} of $CaCO_3$ molecule in the DTPA system. A sharp and high peak intensity occurred at 13.71 for O_1—CO_3 interaction at a distance of 2.25 Å. The O_2—CO_3 and O_3—CO_3 illustrate similar intensity values at 9.07 and 9.05, respectively, at 2.25 Å. The highest intensity of the interaction on Ca^{2+} with CO_3^{2-} is explained by the low metal ion complexes of Ca^{2+} ion in Figure 8 (a), whereby the DTPA molecules exist in the acid form. The low pH values do not effectively chelate metal ions because the hydrogen ions occupy the coordinating functional groups [65]. Aminopolycarboxylic acid chelating agents can most efficiently form complexes with metal ions in alkaline solutions. The surface chelation mechanism, as it pertains to the dissolution of $CaCO_3$, describes the process in which DTPA adsorbs onto the surface of $CaCO_3$ and establishes complexes with calcium ions. This adsorption results in an accelerated dissolution rate. The mechanism follows Langmuir-Hinshelwood kinetics, where the chelating agent attacks the calcium component of the calcite lattice rather than the carbonate component [66].

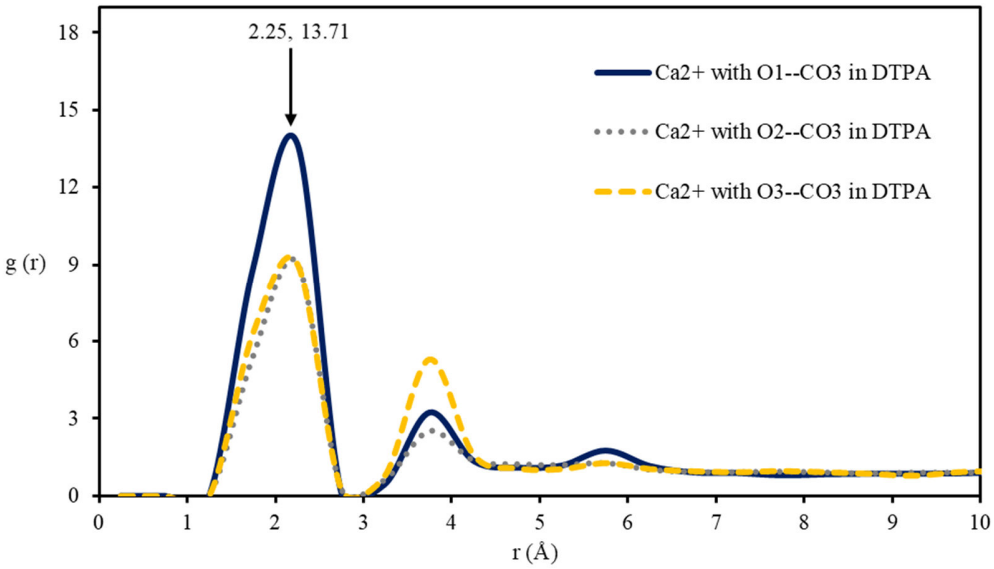

Figure 10. RDF plot of Ca^{2+} and CO_3^{2-} ions interaction that exists in DTPA

Iron with sulphide ions in DTPA

In Figure 11, in separate FeS in DTPA simulation systems, the Fe^{2+}—S^{2-} scale intermolecular interaction in the systems is at 4.75 Å with 2.18 intensity, showing a modest interaction. The interaction between iron ions (Fe^{2+}) and sulphide ions (S^{2-}) in the context of FeS in DTPA primarily involves the complexation of the metal ions by DTPA. The complexation involves binding DTPA carbonyl groups to the iron ions, effectively locking the iron ions within the chelate ring structure of DTPA in Figure 8 (b) [67]. The complexation of iron ions by DTPA prevents the formation of FeS precipitates [68]. The resultant complex between DTPA and iron ions is generally soluble in water, which retains the iron ions in a soluble form, preventing the formation of solid particles and retaining the metal ions in a distributed condition in the solution [69].

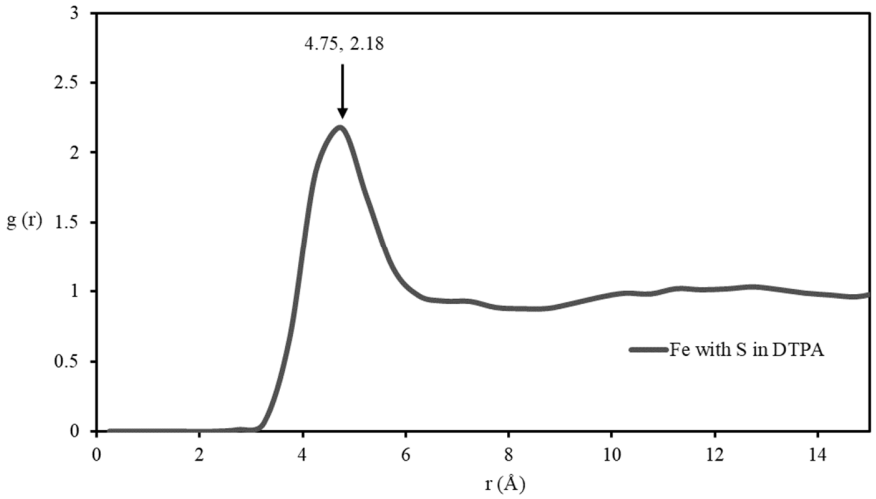

Figure 11. RDF plot of Fe^{2+} and S^{2-} ions interaction that exists in DTPA

Hydrogen in DTPA with (carbonate or sulphide)

Figure 12 (a) depicts the RDFs of hydrogen-atom-containing DTPA molecules in the carboxylic group of DTPA interacting with the carbonate of $CaCO_3$. The H_2 peaks in DTPA have extraordinary intensity values of 11.79 when the distance is 1.25 Å. The positively charged protons (H^+) on DTPA can combine with the negatively charged carbonate ion (CO_3^{2-}) to generate hydrogen carbonate ions (HCO_3^{2-}). This reaction produces hydrogen carbonate ions when the carbonate ion takes up a proton from the DTPA molecule. In summary, the transfer of protons that create hydrogen carbonate ions is the interaction between DTPA and carbonate ions. However, chelating metal ions are the primary function of DTPA. and its interaction with carbonate ions is only a minor aspect of its chemistry.

Figure 12 (b) shows the RDFs of DTPA molecules with hydrogen atoms in the carboxylic group of DTPA with non-metal ions sulphur of FeS interactions. All the peaks show lower probability values of approximately 1.00 with a distance of 3.25 Å. Hydrogen bonding is the mechanism in which the sulphur of FeS and the hydrogen of DTPA interact. There is a chance that the sulphur atom in FeS and the acidic hydrogen atoms in the carboxylic acid groups of DTPA will form hydrogen bonds. However, compared to the coordination bonds that can form between the Fe^{2+} in Figure 8 (b) while the S anion stays constant, the intensity of this interaction in Figure 9 (d) is predicted to be comparatively moderate.

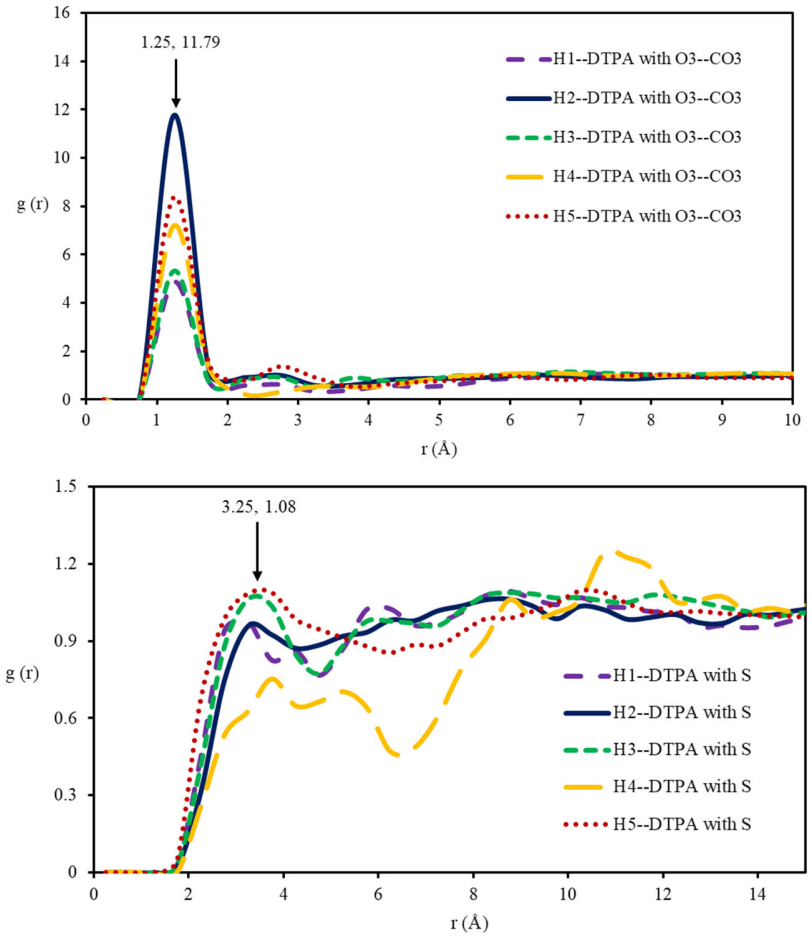

Figure 12. RDF plot for the intermolecular interaction between H in DTPA and (a) O^{2-} in $CaCO_3$ and (b) S^{2-} in FeS

Conclusion

This study elucidates the molecular mechanism of DTPA—H_2O, DTPA—$CaCO_3$—H_2O, and DTPA—FeS—H_2O systems. The analysis of RDF plots for H_2O interactions with hydrogen and oxygen atoms in the DTPA carboxylic groups system reveals strong hydrogen bonding between O—H_2O and H_5—DTPA. The interaction of DTPA—H_2O in the presence of the $CaCO_3$ system modifies the interaction patterns, indicating the interaction shift from water to metal ions. For the DTPA—H_2O in the presence of the FeS system, hydrogen bonding between water and DTPA deteriorates, suggesting the formation of a metal-ligand soluble complex with Fe^{2+} ion. Meanwhile, in the metal ion complexes, DTPA—$CaCO_3$ and DTPA—FeS system interactions show that the carbonyl groups of DTPA exhibit more significant interactions than hydroxyl groups. Amines in DTPA—$CaCO_3$ and DTPA—FeS systems reveal low-intensity interactions, demonstrating a preference for interactions of Ca^{2+} and Fe^{2+} ions with the carbonyl groups of DTPA. The analysis of the amine group in DTPA—CO_3^{2-} and DTP—S^{2-} systems indicates weaker intermolecular interactions, signifying amine preference for Ca^{2+} and Fe^{2+} ions. The ionic interactions within Ca^{2+} and CO_3^{2-} exhibit the highest intensity and shorter radial distance than Fe^{2+} and S^{2-} in the DTPA system. For H—DTPA interactions, H_2—DTPA with O_3—CO_3^{2-} appears expressive, whereas for interactions of H—DTPA with S^{2-}, H_5—DTPA with S^{2-} appears at low intensity. These findings contribute to a better understanding of the chemical processes involved in metal ion complexation (Ca^{2+}/Fe^{2+}) during solid scale dissolution with the chelating agent (i.e., DTPA).

Acknowledgement

The authors express gratitude for the internal grants (RDU 170323 and PGRS 180394) from Universiti Malaysia Pahang Al-Sultan Abdullah.

References

1. Olajire, A. A. (2015). A review of oilfield scale management technology for oil and gas production. *Journal of petroleum science and engineering*, 135: 723-737.
2. Crabtree, M., Eslinger, D., Fletcher, P., Miller, M., Johnson, A., and King, G. (1999). Fighting scale: removal and prevention. *Oilfield Review*, 11(3): 30-45.
3. Vetter, O. J., and Farone, W. A. (1987). Calcium carbonate scale in oilfield operations. In *SPE Annual Technical Conference and Exhibition* (pp. SPE-16908).
4. Vazirian, M. M., Charpentier, T. V., de Oliveira Penna, M., and Neville, A. (2016). Surface inorganic scale formation in oil and gas industry: As adhesion and deposition processes. *Journal of Petroleum Science and Engineering*, 137: 22-32.
5. Nasr-El-Din, H. A., Al-Saiari, H. A., Al-Ruwaily, A. A., and Al-Gamber, S. D. (2006). Field application of emulsified scale inhibitor treatment to mitigate calcium carbonate scale in horizontal wells. In *SPE International Oilfield Scale Conference and Exhibition* (pp. SPE-100456).
6. Adam, F. (2020). Intermolecular interaction of carboxylic group with calcium ions and dissolution of solid scales in Bmim-PF6 and Tba-NfO ionic liquid solution. *Malaysian Journal of Microscopy*, 16(1): 205-216.
7. Mahmoud, M., Hussein, I. A., Sultan, A., Saad, M. A., Buijs, W., and Vlugt, T. J. (2018). Development of efficient formulation for the removal of iron sulphide scale in sour production wells. *The Canadian Journal of Chemical Engineering*, 96(12): 2526-2533.
8. Gamal, H., Abdelgawad, K., and Elkatatny, S. (2019). New environmentally friendly acid system for Iron sulfide scale removal. *Sustainability*, 11(23): 6727.
9. Crabtree, M., Eslinger, D., Fletcher, P., Miller, M., Johnson, A., and King, G. (1999). Fighting scale: removal and prevention. *Oilfield Review*, 11(03): 30-45.
10. Mady, M. F., and Kelland, M. A. (2020). Review of nanotechnology impacts on oilfield scale management. *ACS Applied Nano Materials*, 3(8): 7343-7364.
11. Enyi, G. C., Nasr, G. G., Nourian, A., El Kamkhi, M. A., and Burby, M. L. (2012). Removal of scales in petroleum production tubing utilising high pressure atomisers. ICLASS 2012, 12th Triennial International Conference on Liquid Atomization

and Spray Systems, Heidelberg, Germany.
12. Kamal, M. S., Hussein, I., Mahmoud, M., Sultan, A. S., and Saad, M. A. (2018). Oilfield scale formation and chemical removal: A review. *Journal of Petroleum Science and Engineering*, 171: 127-139.
13. Almubarak, T., Ng, J. H., and Nasr-El-Din, H. (2017). A review of the corrosivity and degradability of aminopolycarboxylic acids. Offshore Technology Conference, Houston, Texas, USA.
14. Hong Ng, J., Almubarak, T., and Nasr-El-Din, H. A. (2018). Low-carbon-steel corrosion at high temperatures by aminopolycarboxylic acids. *SPE Production & Operations*, 33(01): 131-144.
15. Jessop, P. G., Ahmadpour, F., Buczynski, M. A., Burns, T. J., Green Ii, N. B., Korwin, R., Long, D., Massad, S. K., Manley, J. B., Omidbakhsh, O., Pearl, R., Pereira, S., Predale, R. A., Sliva, P. G., VanderBilt, H., Weller. S., and Wolf, M. H. (2015). Opportunities for greener alternatives in chemical formulations. *Green Chemistry*, 17(5): 2664-2678.
16. Mahmoud, M., Abdulraheem, A., Al-Mutairi, S. H., Elkatatny, S. M., and Shawabkeh, R. A. (2017). Single stage filter cake removal of barite weighted water based drilling fluid. *Journal of Petroleum Science and Engineering*, 149: 476-484.
17. Mahmoud, M. A., and Abdelgawad, K. Z. (2015). Chelating-agent enhanced oil recovery for sandstone and carbonate reservoirs. *SPE Journal*, 20(03): 483-495.
18. Sievers, R. E., and Bailar Jr, J. C. (1962). Some metal chelates of ethylenediaminetetraacetic acid, diethylenetriaminepentaacetic acid, and triethylenetetraminehexaacetic acid. *Inorganic Chemistry*, 1(1): 174-182.
19. Sulaiman, M. H., Adam, F., Yaacob, Z., and Noor, Z. M. (2020). Synthesis of ionic salt for calcite and barite solid scale dissolution. *IOP Conference Series: Materials Science and Engineering*, 736(2): 1-6.
20. Sulaiman, M. H., Adam, F., Yaacob, Z., Mohd Noor, M. Z., and Abdullah, N. (2022). Evaluation of carboxylic acid and amine groups with $CaCO_3$, FeS and $BaSO_4$: Molecular dynamic simulations and experimental study. *Arabian Journal for Science and Engineering*, 47(5): 6693-6706.
21. Adam, F., AB, S. H., Yusoff, M. M., and Tajuddin, S. N. (2014). Molecular dynamic simulation of the patchouli oil extraction process. *Journal of Chemical & Engineering Data*, 59(2): 183-188.
22. Allen, M. P., and Tildesley, D. J. (2017). *Computer simulation of liquids*. Oxford University Press.
23. Sun, H., Ren, P., and Fried, J. R. (1998). The COMPASS force field: parameterization and validation for phosphazenes. *Computational and Theoretical Polymer Science*, 8(1-2): 229-246.
24. Lifson, S., Hagler, A. T., and Dauber, P. (1979). Consistent force field studies of intermolecular forces in hydrogen-bonded crystals. 1. Carboxylic acids, amides, and the C: O. cntdot.. cntdot.. cntdot. H-hydrogen bonds. *Journal of the American Chemical Society*, 101(18): 5111-5121.
25. Ghasemi, M., Shafiei, A., and Foroozesh, J. (2022). A systematic and critical review of application of molecular dynamics simulation in low salinity water injection. *Advances in Colloid and Interface Science*, 300: 102594.
26. Hagler, A. T., Lifson, S., and Dauber, P. (1979). Consistent force field studies of intermolecular forces in hydrogen-bonded crystals. 2. A benchmark for the objective comparison of alternative force fields. *Journal of the American Chemical Society*, 101(18): 5122-5130.
27. Chemspider (2023). Pentetic acid.http://www.chemspider.com/ChemicalStructure.2945.html?rid=0b2ec7a4-92a6-4107-94d1-cc18c96ffd9f. [Access online 1 October 2023].
28. Chemspider (2023). Pentapotassium 2,2',2",2"',2""-(1,2-ethanediylnitrilo)pentaacetate http://www.chemspider.com/Chemical-Structure.8342715.html?rid=cade4c9b-3b3e-423b-8388-6e0fd1130002. [Access online 1 October 2023].
29. Chemspider (2023). Calcium carbonate. http://www.chemspider.com/Chemical-Structure.9708.html?rid=0f072ecd-5956-4989-ba07-21c0fe28785a. [Access online 1 October 2023].
30. Chemspider (2023). Iron(II) sulfide. http://www.chemspider.com/Chemical-Structure.8466211.html?rid=cbd8c839-db04-4178-9130-a9c167340863. [Access online 1 October

2023].
31. Chemspider (2023). Water. http://www.chemspider.com/Chemical-Structure.937.html?rid=1fff2418-93ff-47c3-88e0-77180af4730f. [Access online 1 October 2023].
32. Ewald, P. P. (1921). Die Berechnung optischer und elektrostatischer Gitterpotentiale. *Annalen der physik*, 369(3): 253-287.
33. Mudalip, S. K. A., Adam, F., and Bakar, M. R. A. (2019). Evaluation of the intermolecular interactions and polymorphism of mefenamic acid crystals in N, N-dimethyl formamide solution: A molecular dynamics simulation and experimental study. *Comptes Rendus Chimie*, 22(11-12): 771-778.
34. Vatamanu, J., Borodin, O., and Bedrov, D. (2018). Application of screening functions as cutoff-based alternatives to ewald summation in molecular dynamics simulations using polarizable force fields. *Journal of Chemical Theory and Computation*, 14(2): 768-783.
35. Evans, D. J., and Morriss, G. P. (1984). Comment on ‘‘Extensions of the molecular dynamics simulation method. II. Isothermal systems’’. *The Journal of Chemical Physics*, 81(8): 3749-3750.
36. Nosé, S. (1984). A unified formulation of the constant temperature molecular dynamics methods. *The Journal of Chemical Physics*, 81(1): 511-519.
37. Hoover, W. G. (1985). Canonical dynamics: Equilibrium phase-space distributions. *Physical Review A*, 31(3): 1695.
38. Berendsen, H. J. C., Van Gunsteren, W. F., Egberts, E., and De Vlieg, J. (1987). Dynamic simulation of complex molecular systems. Supercomputer Research in Chemistry and Chemical Engineering, ACS Symposium Series; American Chemical Society, Chapter 7:106-122
39. Andersen, H. C. (1980). Molecular dynamics simulations at constant pressure and/or temperature. *The Journal of Chemical Physics*, 72(4): 2384-2393.
40. Romero-Montalvo, E., and DiLabio, G. A. (2021). Computational study of hydrogen bond interactions in water cluster–organic molecule complexes. *The Journal of Physical Chemistry A*, 125(16): 3369-3377.
41. Yoosefian, M., Karimi-Maleh, H., and Sanati, A. L. (2015). A theoretical study of solvent effects on the characteristics of the intramolecular hydrogen bond in Droxidopa. *Journal of Chemical Sciences*, 127:1007-1013.
42. Sandoval, A. A., Sandoval, M. W., Lin, E., and Cheng, K. L. (1970). Hydrogen bonding in some polyaminocarboxylic acids. *Journal of Magnetic Resonance,* 3(2): 258-268.
43. Manning, T. J., and Gravley, E. D. (1995). Protonation sequence study of the solution structure of DTPA by 1H NMR. *Spectroscopy Letters*, 28(3): 291-300.
44. Chen, J., Zheng, Y., Melli, A., Spada, L., Lu, T., Feng, G., ... and Puzzarini, C. (2020). Theory meets experiment for elucidating the structure and stability of non-covalent complexes: Water–amine interaction as a proof of concept. *Physical Chemistry Chemical Physics*, 22(9): 5024-5032.
45. Niu, X., Huang, Z., Ma, L., Shen, T., and Guo, L. (2013). Density functional theory, natural bond orbital and quantum theory of atoms in molecule analyses on the hydrogen bonding interactions in tryptophan-water complexes. *Journal of Chemical Sciences*, 125: 949-958.
46. Yang, B., Ren, P., Xing, L., Wang, S., and Sun, C. (2023). Roles of hydrogen bonding interactions and hydrophobic effects on enhanced water structure in aqueous solutions of amphiphilic organic molecules. *Spectrochimica Acta Part A: Molecular and Biomolecular Spectroscopy*, 296: 122605.
47. Azimi, A. Z. C., Abdullah, N., Adam, F., Hassan, Z., Rahman, S. A., and Noor, M. Z. M. (2023). The simulation of intermolecular interactions of carboxylic and amine groups with calcium carbonate. *Jurnal Teknologi,* 85(1): 91-98.
48. Krishnan, K., and Plane, R. A. (1968). Raman spectra of ethylenediaminetetraacetic acid and its metal complexes. *Journal of the American Chemical Society,* 90(12): 3195-3200.
49. Novak, A., Cotrait, M., Joussot-Dubien, J., and Lascombe, J. (1965). Infrared spectra of and protonation sites in, solid ethylenediaminetetraacetic acid. *Inorganic Chemistry,* 4(5): 767-769.

50. Chapman, D., Lloyd, D. R., and Prince, R. H. (1963). 686. An infrared and nuclear magnetic resonance study of the nature of ethylenediaminetetra-acetic acid and some related substances in solution: hydrogen bonding in α-amino-polycarboxylic acid systems. *Journal of the Chemical Society,* 1963: 3645-3658.
51. Nakamoto, K., Margoshes, M., and Rundle, R. E. (1955). Stretching frequencies as a function of distances in hydrogen bonds. *Journal of the American Chemical Society,* 77(24): 6480-6486.
52. Zhang, H. P., Luo, X. G., Lin, X. Y., Tang, P. P., Lu, X., Yang, M. J., and Tang, Y. (2016). Biodegradable carboxymethyl inulin as a scale inhibitor for calcite crystal growth: molecular level understanding. *Desalination,* 381: 1-7.
53. Chen, H., Guo, Y., Du, Y., Xu, X., Su, C., Zeng, Z., and Li, L. (2021). The synergistic effects of surface functional groups and pore sizes on CO_2 adsorption by GCMC and DFT simulations. *Chemical Engineering Journal,* 415: 128824.
54. Hashim, N. A., Mudalip, S. K. A., Harun, N., Man, R. C., Sulaiman, S. Z., Arshad, Z. I. M., Shaarani, M. S., Azmir, J. (2019). Mahkota dewa Subcritical water extraction process: Experimental and molecular dynamics simulation study. *Chemical Engineering & Technology,* 42(9): 1747-1756.
55. Kundu, S., Ghosh, B., Balasubramanian, S., and Haroun, M. (2011). A biodegradable scale inhibitor for oil well application. *Petroleum Science And Technology,* 29(14): 1512-1520.
56. Bageri, B., Al Jaberi, J., Solling, T. I., Sultan, A., Badhafere, D., and Patil, S. (2023). Evaluating the corrosion index of DTPA at different conditions-key of improving the performance of chelating agents in field treatments. *Geoenergy Science and Engineering,* 223: 211574.
57. Wuyep, E. O., Oluyemi, G. F., Yates, K., and Akisanya, A. R. (2020). Evaluation of interactions between oilfield chemicals and reservoir rocks. *Natural Resources Research,* 29: 1239-1258.
58. Oliveira, R. (1997). Understanding adhesion: a means for preventing fouling. *Experimental Thermal and Fluid Science,* 14(4): 316-322.
59. Eivazihollagh, A., Svanedal, I., Edlund, H., and Norgren, M. (2019). On chelating surfactants: Molecular perspectives and application prospects. *Journal of Molecular Liquids,* 278: 688-705.
60. Xiang, Y., Liu, Y., Mi, B., and Leng, Y. (2014). Molecular dynamics simulations of polyamide membrane, calcium alginate gel, and their interactions in aqueous solution. *Langmuir,* 30(30): 9098-9106.
61. Fredd, C. N., & Fogler, H. S. (1998). The influence of chelating agents on the kinetics of calcite dissolution. Journal of colloid and interface science, 204(1), 187-197.
62. Hassan, A., Mahmoud, M., Bageri, B. S., Aljawad, M. S., Kamal, M. S., Barri, A. A., and Hussein, I. A. (2020). Applications of chelating agents in the upstream oil and gas industry: a review. *Energy & Fuels,* 34(12): 15593-15613.
63. Sajadi, S. A. A. (2010). Metal ion-binding properties of L-glutamic acid and L-aspartic acid, a comparative investigation. *Natural Science,* 2(2): 85.
64. Sosa, R. D., Geng, X., Agarwal, A., Palmer, J. C., Conrad, J. C., Reynolds, M. A., and Rimer, J. D. (2020). Acidic polysaccharides as green alternatives for barite scale dissolution. *ACS Applied Materials & Interfaces,* 12(49): 55434-55443.
65. Fredd, C. N., and Fogler, H. S. (1998). The influence of chelating agents on the kinetics of calcite dissolution. *Journal of Colloid And Interface Science,* 204(1): 187-197.
66. Compton, R. G., and Brown, C. A. (1995). The inhibition of calcite dissolution/precipitation: 1, 2-dicarboxylic acids. *Journal of Colloid and Interface Science,* 170(2): 586-590.
67. Onawole, A. T., Hussein, I. A., Nimir, H. I., Ahmed, M. E., and Saad, M. A. (2021). Molecular design of novel chemicals for iron sulfide scale removal. *Journal of Chemistry,* 2021: 1-11.
68. Almubarak, T., Ng, J. H., Ramanathan, R., and Nasr-El-Din, H. A. (2021). Chelating agents for oilfield stimulation: Lessons learned and future outlook. *Journal of Petroleum Science and Engineering,* 205: 108832.

69. Alhamad, L., Alrashed, A., Al Munif, E., & Miskimins, J. (2020, February). A review of organic acids roles in acidizing operations for carbonate and sandstone formations. *SPE International Conference and Exhibition on Formation Damage Control*, Louisiana, USA.